Direct Detection of Hydrogen Bonds in Monomeric Superoxide Dismutase: Biological Implications†

Lucia Banci,*,‡ Isabella C. Felli,‡ and Rainer Kümmerle‡,§

Magnetic Resonance Center (CERM), University of Florence, Via Luigi Sacconi 6, 50019 Sesto Fiorentino, Italy, and Bruker Italiana srl, Via Pascoli 70/3, 20133 Milano, Italy

Received August 6, 2001; Revised Manuscript Received November 21, 2001

ABSTRACT: Hydrogen bonds were directly determined via NMR with different experimental approaches at 600 and 800 MHz for reduced monomeric superoxide dismutase (Q133M2SOD, 16 kDa). This protein contains a copper and a zinc ion and shows the classical superoxide dismutase (SOD) eight-stranded β-barrel fold. The best results for this intermediate molecular mass protein were obtained using a TROSY version of the long-range HNCO experiment at high magnetic field (800 MHz) or with a cryoprobe at 600 MHz. The backbone hydrogen bond network that defines the secondary structure of the protein was detected. Thirty-five backbone hydrogen bonds were identified. The lower limit for their detection, their relation to the TROSY R_2 rates, and the correlation between hydrogen bond detectability and signal line width are discussed. Experiments were also optimized to detect hydrogen bonds involving key side chains, which lead to the observation of five hydrogen bonds. In particular, the hydrogen bonds involving the side chain of Asp 124 were observed, which show significant differences with respect to the bonds expected on the basis of the crystal structure. The relevance of this finding relies also on the fact that Asp 124 is a key residue in determining the affinity of the protein for zinc. It has now been determined that the gain of the toxic function of peroxynitrite formation in SOD mutants related to amyotrophic lateral sclerosis (ALS) is due to SOD species lacking the zinc ion, as a consequence of a reduced affinity for zinc. Therefore, this study provides structural hints for understanding the origin of the enzymatic behavior of the Zn-deficient SOD.

It has long been recognized that hydrogen bonds play an important role in structural biology. Their energy (2−20 kJ/mol), intermediate between that of a covalent bond (100−600 kJ/mol) and weaker interactions such as van der Waals interactions, lies in the perfect range for stabilizing three-dimensional (3D) folds as well as triggering macromolecular functions and interactions. For example, the network of hydrogen bonds is the primary determinant of the secondary structure of proteins and is responsible for the DNA/RNA base paring. Formation or breaking of hydrogen bonds is one of the mechanisms used by enzymes to catalyze reactions in biological systems.

NMR[1] can contribute to the characterization of hydrogen bonds through several observables such as reduced solvent exchange rates and changes in chemical shifts and fractionation factor (*1*). However, these parameters do not directly indicate the nature of the two residues involved in the hydrogen bonding interaction; rather, they are inferred from the 3D structure, if available. The partial nature of the bond gives rise to a weak scalar *J* coupling between the nuclear spins of the two interacting moieties. Indeed, this has stimulated the development of several new experiments, initially in nucleic acids (*2*, *3*), for directly determining the two partners in a hydrogen bond (*4*). Hydrogen bond-mediated *J* couplings in proteins are very small (<2 Hz). Therefore, the main problem for NMR experiments is sensitivity. The direct detection of hydrogen bonds has been reported for proteins with molecular masses of <10 kDa (*5*−*7*) and on a 30 kDa fully deuterium-labeled protein (*8*). In the first case, experiments with completely decoupled ^{1}H−^{15}N multiplet components were used (*5*−*7*) (long-range HNCO). However, the detection of hydrogen bonds in the second case was only possible with a TROSY-like approach (*9*) in which only the sharpest component of the ^{1}H−^{15}N multiplet is preserved throughout the experiment and subsequently detected (*8*) (long-range TROSY HNCO). Since hydrogen bond detection strongly depends on relaxation rates of ^{15}N magnetization, it is not evident a priori which of the approaches would be the most appropriate for a medium-sized protein such as monomeric superoxide dismutase (16 kDa).

Superoxide dismutase (SOD) is an essential enzyme for living organisms. SOD catalyzes the dismutation of a superoxide anion, a radical that can be produced during

† Financial support of the EU through contract HPRI-CT-1999-00009 is gratefully acknowledged. This work has been also partly supported by MURST ex 40% 1999 (Italy).

* To whom correspondence should be addressed: Magnetic Resonance Center (CERM), University of Florence, Via Luigi Sacconi, 6, 50019 Sesto Fiorentino, Italy. Phone: +39055 4574263. Fax: +39055 4574253. E-mail: banci@cerm.unifi.it.

‡ University of Florence.

§ Bruker Italiana srl.

[1] Abbreviations: ALS, amyotrophic lateral sclerosis; CSI, chemical shift index; HSQC, heteronuclear single-quantum spectroscopy; INEPT, insensitive nuclei enhanced by polarization transfer; NMR, nuclear magnetic resonance; SOD, superoxide dismutase; TROSY, transverse relaxation optimized spectroscopy; WT, wild type.

10.1021/bi011617b CCC: $22.00
Published on Web 02/08/2002

respiration and photosynthesis as a side product of dioxygen reduction (*10*−*12*). The enzymatic mechanism of superoxide dismutation into oxygen and hydrogen peroxide follows a two-step cycle (*13*, *14*):

$$Cu^{2+} + O_2^- \rightarrow Cu^+ + O_2$$

$$Cu^+ + O_2^- \rightarrow Cu^{2+} + H_2O_2$$

The eukaryotic enzymes are homodimeric with a large interface of alternating hydrophilic and hydrophobic interactions (*15*, *16*). Each subunit contains a copper and a zinc ion bridged by a histidinate ring (His 63), which coordinates both metal ions. The coordination sphere is completed by an additional three histidines for the copper ion (His 46, 48, and 120) and by two histidines and one aspartate for the zinc ion (His 71 and 80 and Asp 83) (*16*). Monomeric species have been obtained by mutating a few hydrophobic residues within the dimerization domain to hydrophilic, charged residues (*17*, *18*). The structure and dynamic properties of this monomeric SOD have been previously reported (*19*−*21*). In the study presented here, we report a direct determination of the hydrogen bonding networks present in the reduced form of a monomeric SOD where Phe 50 and Gly 51 have been substituted with glutamates (*17*). Furthermore, a negative residue, Glu 133, present in the active site channel has been mutated to a neutral Gln (*18*) to partially recover the enzymatic activity, which is drastically reduced in the monomeric species. The monomeric species investigated in this study (Q133M2SOD hereafter) has been extensively characterized through both X-ray (*22*) and NMR (*19*) (structure and dynamics) in addition to enzymatic activity assays.

Herein we report the direct determination through NMR of backbone and side chain hydrogen bonds to (1) assess whether this is feasible for a non-perdeuterated medium-sized protein, (2) incorporate them in structure calculations, and (3) identify and characterize key hydrogen bonds of catalytic mechanistic importance.

EXPERIMENTAL PROCEDURES

Sample Preparation. The monomeric mutant of human SOD (Q133M2SOD) has been expressed, as previously described (*18*), by replacing two hydrophobic residues at the interface (Phe 50 and Gly 51) with two hydrophilic Glu residues and introducing an additional mutation (Glu → Gln) at position 133 (*19*, *23*, *24*). Protein samples enriched in ^{13}C and ^{15}N were isolated and purified as previously described (*23*). The copper and zinc content was checked through atomic absorption. A 2 mM protein sample in phosphate buffer at pH 5.0 with 10% D_2O was reduced with ascorbate (final concentration of 4.0−6.0 mM) under an argon atmosphere and was used for NMR experiments.

NMR Experiments. NMR experiments were carried out with Bruker Avance 600 and 800 MHz NMR spectrometers both equipped with a ^1H, ^{13}C, ^{15}N TXI probe with a self-shielded *z*-gradient coil. Once the parameters were optimized, the final experiments were also performed on a Bruker Avance 600 MHz spectrometer equipped with a cryoprobe. The pulse sequence that was used is a modification of the HNCO sequence (*25*−*27*) with sensitivity enhancement for NH detection (*28*). Different versions of the experiment, either with $^1H-^{15}N$ multiplet decoupling or without it to obtain a TROSY-like pattern (*8*), were performed. To quantify $^{3h}J_{NC'}$ couplings, we modified the latter experiment (TROSY-like pattern) according to the method of Cordier and Gresziek (*5*) (see also the Supporting Information). TROSY R_2 relaxation experiments, which measure the transverse relaxation rate of the sharper component of the doublet (with R_2 being the relevant parameter with respect to the long-range TROSY-HNCO experiment), were carried out to estimate the detection limit for hydrogen bond scalar couplings. All triple-resonance experiments were carried out in the two-dimensional (2D) $^1H-^{13}C$ version. The long-range HNCO experiments, for detecting hydrogen bonds involving backbone NH groups, were carried out with sweep widths of 20 and 16 ppm for the ^1H and ^{13}C dimensions, respectively. The $^1H-^{15}N$ INEPT transfer delays were set to 2.3 ms. The ^1H, ^{13}C, and ^{15}N carriers were placed at 4.69, 173, and 120 ppm, respectively. Selective carbonyl ^{13}C pulses were given with G3 and G4 shapes (*29*). The prescan delay was 1.3 s. One reference experiment for detecting one-bond HNCO connectivities was carried out with an N−C′ INEPT transfer delay of 24 ms with 16 scans and 2048 × 128 complex data points for a duration of 105 min. The long-range (TROSY) HNCO experiment, optimized for detecting hydrogen bonds between backbone nuclei, was carried out with an INEPT transfer delay of 133.2 ms. The latter experiment was carried out with 68 complex increments, 1024 scans each, for a total duration of 75 h. Composite pulse decoupling of ^{15}N resonances was carried out during acquisition only during the fully decoupled experiment with an RF field of 1.5 kHz.

Quantification of the $^{3h}J_{NC'}$ coupling constants was carried out at 800 MHz by shifting the two $^{13}C'$ inversion pulses during the NC′ inept transfer step to obtain evolution of the sequential NC′ coupling for 16.5 ms [$=1/(2J_{NC'})$] while keeping the relaxation delays constant (see also the Supporting Information). Compared to the original experiment where the inversion pulses were shifted by 16.5 ms [$=1/(2J_{NC'})$], our approach minimizes errors for nonuniform sequential $J_{NC'}$ coupling constants.

An additional experiment was optimized for detecting hydrogen bonds involving histidine side chains. The two main parameters that needed to be optimized were the ^{15}N and ^{13}C pulses. The ^{15}N carrier was moved to 170 ppm, a typical chemical shift for ^{15}N histidine side chain nuclei, and the ^1H carrier was placed around 10−12 ppm, the average chemical shift for histidine side chain NH groups. ^{13}C carbonyl pulses were made selective for histidine side chain carbon spins to avoid evolution of the antiphase coherence between intraring N and C, which would cause a significant loss of signal intensity. Q3 and Q5 selective pulses (*30*) were used to irradiate C′ spins and to avoid inversion of aromatic histidine carbon spins. The ^1H sweep width was 14 ppm with the ^1H carrier placed at 12 ppm. All the other parameters were the same as described above.

Data were processed with the Bruker Xwin-NMR 2.6 software with several different parameters to better evaluate results.

Structure Calculations. The calculation protocol, using the program DYANA (*31*), and all the input files were identical to the ones used for the original solution structure calculations (*19*) except for the inclusion of hydrogen bonds. The latter

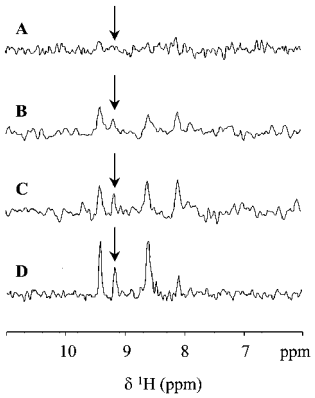

FIGURE 1: One-dimensional (1D) traces at 172.3 ppm (^{13}C′ chemical shift) along the ^{1}H dimension of four different 2D ^{1}H−^{13}C experiments to detect hydrogen bonds: (A) 600 MHz long-range HNCO, (B) 600 MHz long-range TROSY HNCO, (C) 800 MHz long-range TROSY HNCO, and (D) 600 MHz cryoprobe long-range TROSY HNCO. The cross-peak at 9.17 ppm denoted with an arrow is visible only with the TROSY approach and is assigned to the NH 95−CO 35 hydrogen bond.

were included as structural constraints by imposing a lower distance limit of 2.6 Å for the N−O distance and two upper distance limits for the H^N−O and N−O distances of 2.4 and 3.3 Å, respectively. To estimate the effect of hydrogen bond constraints on the structure's precision and accuracy, the calculations were repeated with and without hydrogen bond constraints. The 30 structures with the lowest target function (*31*), after annealing 400 randomly generated structures, constituted the final family of structures.

The quality of the structures was evaluated in terms of deviations from ideal bond lengths and bond angles and through Ramachandran plots obtained with the programs PROCHECK (*32*) and PROCHECK-NMR (*33*). Structure calculations were carried out on a Linux cluster.

RESULTS

NMR Spectroscopy. A comparison of the experiments carried out at 600 MHz with and without the TROSY approach (Figure 1A,B) shows that also for a medium-sized protein like Q133M2SOD with a molecular mass of 16 kDa, the TROSY-like approach yielded a significant improvement. Indeed, in the fully decoupled long-range HNCO, in addition to the sequential HNCO cross-peaks that are not completely suppressed, connectivities due to small intraresidue couplings ($^3J_{HNC\gamma}$) could be unambiguously detected only for residues Asn 65, Asp 96, Asp 101, Asp 124, and Asn 131. These cross-peaks facilitate the assignment of side chain carbonyl and carboxyl atoms. Furthermore, only three cross-peaks arising from hydrogen bonds were above the noise level of this experiment. The long-range TROSY HNCO, which yields a TROSY-like pattern, gives instead a spectrum with a significantly increased signal-to-noise ratio (S/N) and 12 detectable backbone hydrogen bonds. A comparison of a single cross section from the two experiments is shown in panels A and B of Figure 1. Thus, the TROSY approach was much better suited to identifying hydrogen bonds in medium-sized proteins, due to the long delays present in the pulse sequence. The experiments were then repeated at 800 MHz to take further advantage of the TROSY approach. For comparison, the same slice as in Figure 1B is reported in Figure 1C and a portion of the 2D spectrum is shown in

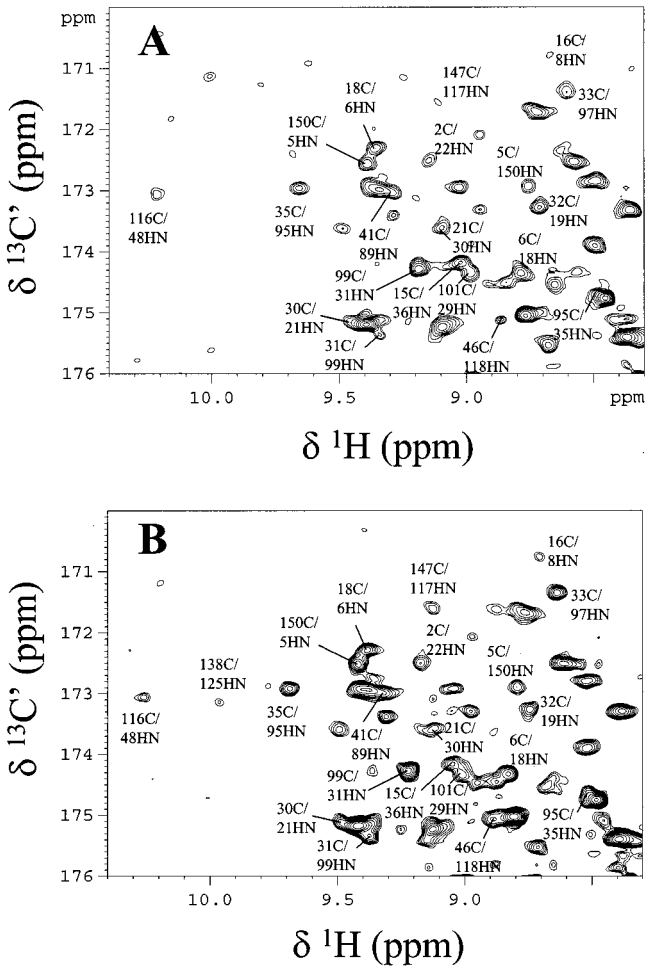

FIGURE 2: Part of the 2D ^{1}H−^{13}C maps acquired for detecting hydrogen bonds with long-range TROSY HNCO at 800 MHz (A) and at 600 MHz using a cryoprobe (B). Only cross-peaks arising from hydrogen bond interactions are labeled.

Figure 2A. Cross-peaks due to hydrogen bonds are labeled with their assignment. Since the main problem in hydrogen bond detection is the inherent low sensitivity of the experiment, data were also collected with a cryoprobe at the highest magnetic field for which it was available at the time of the experiments (600 MHz). Indeed, taking into account the slightly different acquisition parameters, we obtained a factor of approximately 2 in S/N compared to that from the experiment at 800 MHz, consistent with the higher sensitivity of such a probe. Figure 2B shows the same region of the spectrum acquired with the cryoprobe, and the cross section is presented in Figure 1D.

Coupling constants could be quantified for 71% of the backbone hydrogen bonds ranging from −0.3 to −1.2 Hz (Supporting Information). The smallest observed $^{3h}J_{NC'}$ coupling constant was −0.3 Hz for a residue with a TROSY R_2 relaxation rate of approximately 10 Hz (see the Supporting Information). The $^{3h}J_{NC'}$ lower limit increases with increasing TROSY R_2 relaxation rates. This is the case for most residues in the loop regions (see the Supporting Information), justifying the absence of strong hydrogen bonds for residues in these regions.

The available assignments of Q133M2SOD (*23*) were used to identify connectivities arising from hydrogen bonds between backbone atom pairs. The hydrogen bonds experimentally detected through NMR are reported in Table 1. For

Table 1: Backbone Hydrogen Bonds Directly Detected in Solution with Long-Range TROSY HNCO on Q133M2SOD (third column, HNCO) and Those Predicted[a] from the Available Solution (*19*) (fourth column, NMR) and Solid State (*22*) Structures (fifth column, X-ray)

donor (HN)	acceptor (O)	HNCO[b]	NMR[c]	X-ray
Thr 2	Gln 22			X
Ala 4	Phe 20	X	100	X
Val 5	Gly 150	X		X
Ala 6	Ile 18	X	100	X
Leu 8	Gly 16	X	100	X
Lys 9	Cys 146	X	94	X
Gln 15	Lys 36		82	X
Gly 16	Leu 8		100	X
Ile 18	Ala 6	X	100	X
Asn 19	Trp 32	X	100	X
Phe 20	Ala 4	X	100	X
Glu 21	Lys 30	X	100	X
Gln 22	Thr 2	X		X
Gly 27	Glu 24	X		X
Val 29	Asp 101	X	100	X
Lys 30	Glu 21	X	100	X
Val 31	Ile 99	X	100	X
Trp 32	Asn 19	X	100	X
Gly 33	Val 97		100	X
Ile 35	Ala 95	X	100	X
Lys 36	Gln 15	X	100	X
Gly 37	Gly 93		100	−
Leu 38	Gly 93	*	71	X
Gly 41	Ala 89	X	94	X
His 43	Val 87	X	82	X
Gly 44	Lys 122	*	100	X
Phe 45	Gly 85		100	X
His 46	Val 118	X	100	X
Val 47	Gly 82		88	X
His 48	Thr 116	X	100	X
Glu 49	Pro 62	X	100	X
Glu 50	Ala 60			X
Thr 54	Asp 52			X
Thr 58	Ala 55			X
Phe 64	Val 47		59	X
Ser 68	Asn 65			X
His 71	Thr 135		100	X
Asp 76	Gly 73		100	X
Gly 82	Phe 64			X
Asp 83	His 80			X
Gly 85	Asp 83		94	−
Val 87	His 43	X	100	X
Ala 89	Gly 41	X	88	X
Asp 90	Val 94	X	100	X
Gly 93	Asp 90		100	X
Ala 95	Ile 35	X		X
Val 97	Gly 33	X	100	X
Ile 99	Val 31	X	100	X
Asp 101	Val 29	*	100	X
Ser 111	Gly 108			X
Ile 112	Ser 105		100	X
Gly 114	Ile 149	*		X
Arg 115	Ile 112		77	X
Thr 116	His 48	X		X
Leu 117	Gly 147	X	100	X
Val 118	His 46	X	100	X
Val 119	Ala 145			X
Glu 121	Ser 142		94	X
Lys 122	Ala 140		71	X
Asp 125	Gly 138	X	100	X
Lys 128	Asp 125		94	X
Thr 135	Glu 132			X
Lys 136	Gln 133			X
Thr 137	Gln 133	X	100	X
Gly 138	Ser 134			X
Leu 144	Val 119			X
Cys 146	Lys 9	*	100	X
Gly 147	Leu 117		100	X
Ile 149	Arg 115	X		X
Gly 150	Val 5	X		X
Ala 152	Lys 3			X

[a] The presence of a hydrogen bond was determined, through the MOLMOL program (*41*), using a threshold of 2.5 Å for the H^N-O distance (r_{H^N-O}) and an angle of 35° between the HN and CO vectors ($\theta_{H^NN-C'O}$). [b] X, unambiguously assigned; *, cross-peaks in overlap. [c] Percentage of structures (of the 17-structure family) showing the corresponding hydrogen bond.

Table 2: Side Chain Hydrogen Bonds Directly Detected in Solution with Optimized Long-Range TROSY HNCO on Q133M2SOD (third column) and Those Predicted from the Available Solution (*19*) (fourth column) and Solid State (*22*) Structures (fifth column)[a]

donor	acceptor	HNCO[b]	NMR[c]	X-ray[d]
Asn 86 HD22	Asp 124 O			X
Asn 131 HD22	Asn 131 O		100	
Asn 139 HD21	Asp 125 OD2			X
Asn 139 HD22	Asn 131 OD1	*		X
Gln 22 HE21	Gly 27 O	X		X
Glu 24 NH	Gln 22 OD1	X		
His 43 HD1	His 120 O	X	94	X
His 46 HE2	Asp 124 OD2		82	X
His 48 HD1	Gly 61 O		100	
His 71 HE2	Asp 124 OD1	X	71	X
His 120 HD1	Gly 141 O		82	X
His 120 HD1	Ser 142 O			X
Leu 126 NH	Asp 124 OD1	X		

[a] The hydrogen bonds were predicted through the MOLMOL program (*41*) using a threshold of 2.5 Å for the H^N-O distance (r_{H^N-O}) and an angle of 35° between the HN and CO vectors ($\theta_{H^NN-C'O}$). Only hydrogen bonds that can be detected through the experiments that were performed (NH as the donor in His, Asn, and Gln and CO as the acceptor in Asn, Gln, Asp, and Glu) are shown in the table. [b] X, unambiguously assigned; *, signals in overlap. [c] H-Bonds predicted under the above-mentioned conditions in the percentage of the 17 structures of the family used for the prediction. [d] X, predicted under the above-mentioned conditions.

comparison, hydrogen bonds predicted on the basis of the available solution (*19*) and solid state (*22*) three-dimensional structures are also reported.

In addition to backbone hydrogen bonds, the HNCO experiment can provide information about hydrogen bonds between NH groups and carbonyls of protein side chains. However, while backbone $^{15}N(H)$ and $^{13}C(O)$ resonances are each characterized by very similar NMR parameters (chemical shifts and coupling constants), much larger variability for side chains is observed. Therefore, detection of hydrogen bonds involving side chains, which can be very relevant for the biological function, requires carefully optimized experiments. The protein side chains with the parameters most similar to those of the backbone are aspartate, glutamate, asparagine, and glutamine. Hydrogen bonds involving a carbonyl (asparagine and glutamine) or a carboxyl (aspartate and glutamate) should thus be detectable with the standard experiment in addition to those involving an NH_2 group, provided the experiment is set up in such a way to observe the NH_2 group itself, which is the case for the experiment used here. Experimentally observed hydrogen bonds involving side chains are reported in Table 2.

Hydrogen bonds involving the NH group of histidine side chains are relevant as they provide structural information about the imidazole ring and about their interactions. They, however, cannot be easily detected with the same experimental setup as that used to detect backbone hydrogen bonds due to the very different NMR parameters characterizing the $^{15}N(H)$ histidine side chain with respect to the peptide $^{15}N(H)$. Thus, a specifically optimized HNCO experiment is necessary to detect these couplings. The experiment optimized for histidines allowed us to detect one very clear hydrogen bond between His 43 HD1 and His 120 CO. A weak peak corresponding to the hydrogen bond between His 71 HE2 and Asp 124 CO was also observed (Table 2).

Overall, 35 hydrogen bonds involving two backbone nuclei (backbone H-bonds, Table 1) and five hydrogen bonds

involving at least one side chain nucleus (side chain H-bonds, Table 2) were detected.

Structure Calculations. The solution structure calculations of monomeric SOD were performed using, as experimental constraints, the distance limits derived from NOEs and the dihedral angle constraints derived from ^3J coupling constants used in previous calculations (*19*).

To evaluate selectively the contribution to the overall definition and quality of the structure of the experimentally detected hydrogen bonds, the calculations were repeated with and without the inclusion of 40 hydrogen bonds as structural constraints. The family of structures calculated using the experimentally detected hydrogen bonds as structural constraints exhibits essentially the same average rmsd values (1.06 ± 0.17 to 1.01 ± 0.16 for the backbone and 1.66 ± 0.16 to 1.61 ± 0.15 for all heavy atoms) and a slight increase in the total target function (from 2.01 ± 0.12 to 2.35 ± 0.13 Å^2). This is expected since in this case, the solution structure is already well defined by an average of 13.8 meaningful constraints per residue (*19*), of which the hydrogen bonds represent only a small fraction. However, the structure is improved in terms of accuracy; the hydrogen bond constraint deviation in the structures calculated without them is 18.72 ± 9.00 Å^2, while it drops to 0.9 ± 0.10 Å^2 when experimentally detected hydrogen bonds are included in the calculations. These values show the better accuracy of the newly calculated structure and indicate that hydrogen bond constraints are consistent with other types of structural constraints. The rmsd per residue within each family of structures and between the two average structures shows a slight local decrease for residues where hydrogen bonds were included, but no significant differences, in most cases, for the final conformation.

DISCUSSION

Hydrogen bonds are quite important in determining the three-dimensional structure and function of a protein. Direct detection of hydrogen bonds through NMR represents an extremely powerful tool as it can be achieved in the very early stages of the process leading to structure calculations. For backbone hydrogen bonds, their identification requires only backbone assignments and provides immediate information regarding the type of protein fold. The experimentally detected backbone hydrogen bonds for Q133M2SOD are reported, versus residue number, in Figure 3. Eight counterdiagonal patterns characteristic of antiparallel β-strands can be noted, arising from the conserved eight-stranded β-barrel present in all known SOD structures, which has further only a single short α-helix spanning residues 133−138. The determination of secondary structural elements, in the case of an unknown protein, is quite valuable information that may allow the immediate discrimination between different types of protein folds.

Hydrogen bonds can then be used as constraints in solution structure calculations, providing medium- to long-range structural information. In the solution structure calculations of Q133M2SOD (*19*), in addition to improving the overall accuracy of the structure, the hydrogen bond constraints increased the precision of some key side chains (see below). Furthermore, hydrogen bonds should significantly speed the process of structure calculations when they are performed with a reduced set of constraints, particularly when used in conjunction with other easily available constraints such as CSI, pseudocontact shifts, residual dipolar couplings, etc.

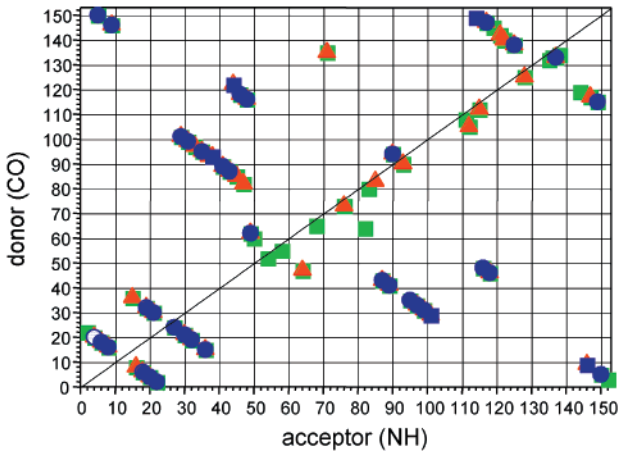

FIGURE 3: Two-dimensional plot representing hydrogen bond correlations experimentally detected through long-range TROSY-HNCO experiments and those predicted on the basis of the X-ray structure (square) and the NMR structure (triangle). Also, the five ambiguous connectivities are shown as blue squares. Only backbone H-bonds are reported.

As the structure of Q133M2SOD has been determined also via X-ray crystallography (*22*), it is interesting to compare the hydrogen bonds predicted from the crystal structure with those directly detected in solution (Figure 3 and Table 1). Although a direct correlation between predicted and experimentally observed hydrogen bonds was evident for the first segment of the protein (residues 4−50), most of the hydrogen bonds predicted from both the X-ray and solution structures were not directly detected in the loop regions. These nondetected hydrogen bonds are located in loop IV (residues 48−85), loop VI (residues 102−114), and loop VII (residues 120−144). These loops exhibit conformational heterogeneity in solution (*19*, *21*, *23*) and solid state (*22*, *34*) structures.

For example, it has been noted in the recently reported X-ray structures of bovine CuZn SOD (*34*) that the two subunits crystallize in different conformations, one of which is characterized by temperature factors for the loop regions that are much higher than those for the other (especially for residues 121−144) (*34*). This finding is in agreement with the conformational exchange processes of loop regions. In the solid state, the observed conformation may have been obtained by "freezing out" during the crystallization process, essentially trapping one of the many accessible conformations for these loops (*22*). Direct evidence of conformational exchange equilibria in loop regions, which results in rmsd values that are larger than the average for these regions (especially for residues 49−62 and 63−84) (*19*), has been provided through ^{15}N relaxation measurements (*21*). Carbonyls of residues 57, 58, and 61 escape detection (*23*), which may be the consequence of extensive conformational exchange contributions to transverse relaxation. In the work presented here (data not shown), an exchange process involving the aromatic ring of His 48 (His 48 Nδ_1), which is very close to the carbonyl of Gly 61, has been detected through HSQC experiments carried out at different temperatures. Conformational exchange processes in these loop regions are a consequence of their surface location. Loops IV and VI are structurally and functionally important as they

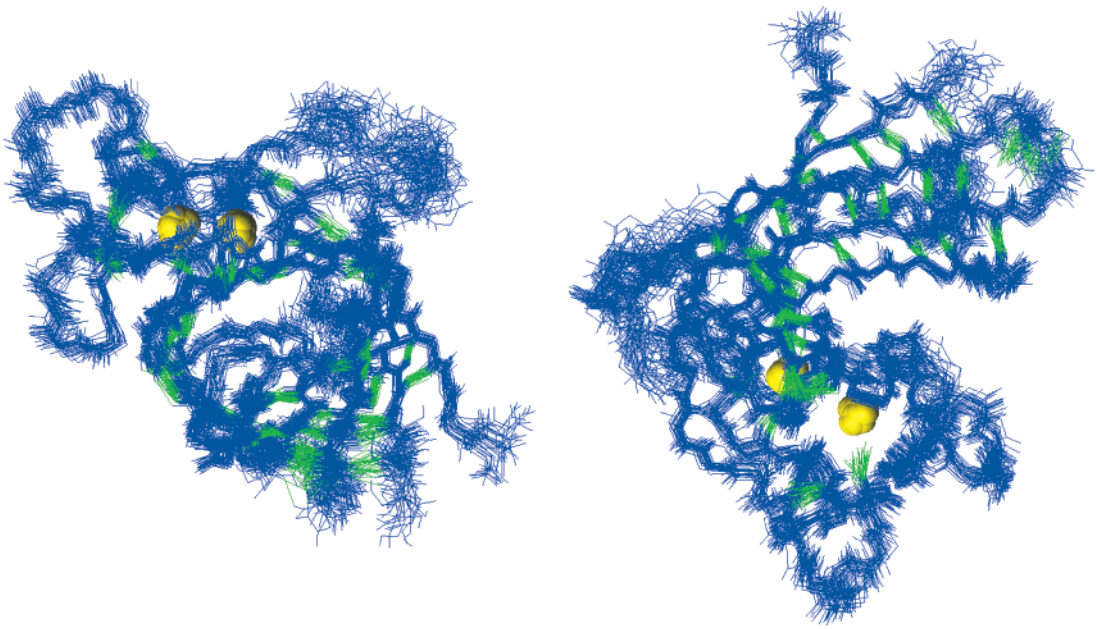

FIGURE 4: Two different views of the NMR solution structure of Q133M2SOD after inclusion of experimentally detected hydrogen bonds as structural constraints. The hydrogen bonds detected experimentally are shown as green bars. The two metal ions are shown in yellow.

form the channel to the active site. The accessibility at room temperature of more than one conformation contributes to the increase in the level of diffusion of superoxide anion to the active site.

If exchange between different conformations involving hydrogen bonds occurs, then these hydrogen bonds are present only part of the time. This undermines direct determination of hydrogen bonds in solution, as this relies on very small effects ($|^{3h}J_{NC'}| \approx 0.2-1$ Hz) that may be easily averaged out by motions. On the other hand, direct detection proves the presence of a stable hydrogen bond in solution. The few hydrogen bonds identified in the loop regions must therefore have important structural effects. The NH 49−CO 62 hydrogen bond stabilizes the two edges of the first part of loop IV immediately prior to the ligand His 63; the NH 125−CO 138 hydrogen bond is important for the backbone arrangement around the metal binding site, and the NH 44−CO 122 hydrogen bond connects the latter to the β-barrel. All these hydrogen bonds form a network of interactions that stabilizes the metal binding region. The hydrogen bond between NH 137 and CO 133 is consistent with their location in the short α-helix.

Three of these side chain hydrogen bonds (Table 2) involve residues in the β-barrel (Gln 22 HE21−Gly 27 CO, Glu 24 NH−Gln 22 OD, His 43 HD1−His 120 CO). The first two hydrogen bonds are located on a surface loop. Interestingly, the hydrogen bond between Glu 24 NH and Gln 22 OD1 is not predicted from either the X-ray or the solution structure (Table 2). However, the His 43 HD1−His 120 CO hydrogen bond is observed in solution and solid state SOD structures. This is a key hydrogen bond as it anchors the metal binding His 120 to the β-barrel.

In the loop regions, two hydrogen bonds involving the carboxylate of Asp 124 have been identified (Table 2). Asp 124 has been claimed, since the first SOD three-dimensional structure was determined (*15*), to be important in establishing a "second-sphere" bridge between the two metal ions by forming hydrogen bonds between the carboxylate group and the imidazole rings of His 71 (coordinated to Zn) and His 46 (coordinating Cu). The importance of this conserved residue on the structural and biological properties of SOD has been shown through mutagenesis; i.e., the replacement of Asp 124 with a Gly residue, whose side chain obviously cannot form any hydrogen bond, produces a derivative which has a very low affinity for zinc (the expressed protein has only 5% zinc content) and which retains at most 50% activity (*35*). Being located in an intermediate position between the two metal sites, the Asp124Gly mutation dramatically influences the stability of the zinc site while it does not appreciably affect the stability of the copper site. The hydrogen bonds we observe in solution in the reduced state may provide an explanation for this specificity. In solution, the carboxylate group of Asp 124 forms two hydrogen bonds. One hydrogen bond is with HE2 of His 71, and one is with NH of Leu 126. No hydrogen bond with the His 46 ring is detected, despite the fact that such connectivity should fall in a "clean" region of the spectrum.

Inclusion of these hydrogen bonds in structure calculations produces a more defined conformation of the side chain of Asp 124 (Figure 5A,B), which is not determined by any other long-range structural constraint. The refined solution structure clearly shows that the side chain of Asp 124 points toward the backbone of Leu 126 and toward the zinc site, being between residues 126 and 71, and away from His 46 (a copper ligand) (Figure 5B). The Asp 124 side chain assumes a very similar orientation in all the available X-ray structures of dimeric human SOD (Figure 5C). The conformation of the side chain of Asp 124 in the crystal is characterized by the presence of three hydrogen bonds with the two histidine rings as well as with Leu 126. Careful inspection of the relevant distances and angles in the crystal structure (PDB entry 1mfm) actually suggests that the His 46−Asp 124 hydrogen bond is stronger than the His 71−Asp 124 bond. The absence of the former and the direct detection of the latter hydrogen bond in our long-range TROSY-HNCO experiments establish that, in the reduced protein in solution,

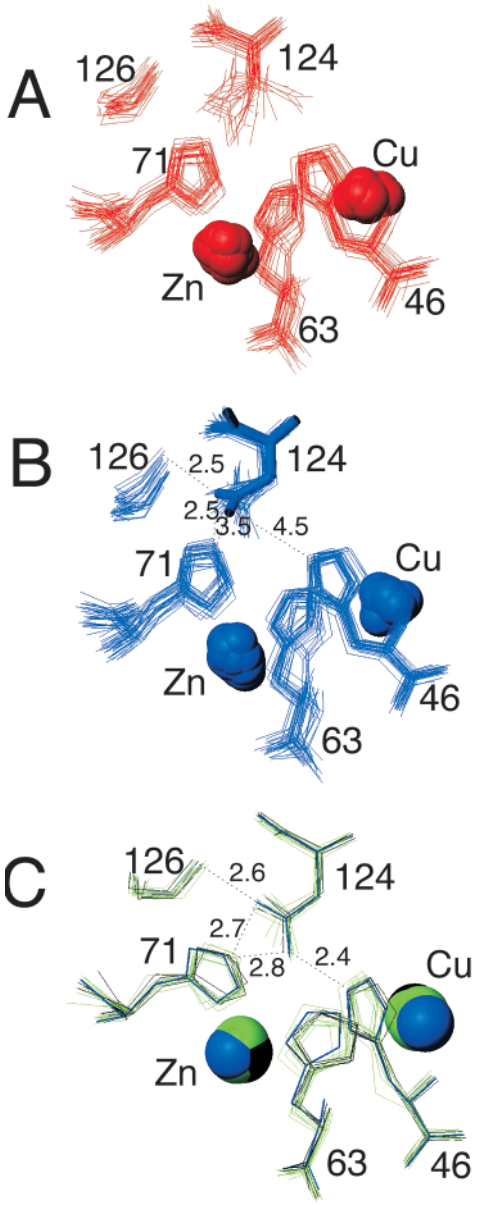

FIGURE 5: Closeup view of the metal binding sites, showing the side chain of Asp 124, the backbone of residue 126 (left), and metal ligands 46, 63, and 71. Panels refer to the NMR solution structure of Q133M2SOD calculated without (A) and with (B) experimentally detected hydrogen bonds and to the available X-ray structures [PDB entry 1sos (black), PDB entry 1fun (green), and PDB entry 1mfm (blue)] of human SOD (C). The orientation displayed for this Asp side chain in the solid state is the same for the bovine isoenzyme (both oxidized and reduced, data not shown).

the carboxylate of Asp 124 has a different conformation, pointing toward the zinc binding site. This suggests the structural rationale for the reduced affinity for Zn in the Asp124Gly mutant (*35*). Indeed, when Asp 124 is converted into a Gly, and therefore no carboxylate is available to be hydrogen-bonded to the Zn-coordinating His, the protein is expressed without zinc. Therefore, Asp 124 is responsible for preorganizing the zinc site, thus determining the optimal conformation for receiving the zinc ion.

The present characterization (and the improvement of experiments for side chain hydrogen bond detection) may be relevant for understanding the basis of the "gained activity" present in the amyotrophic lateral sclerosis (ALS)-related SOD mutants (*36*−*38*). It has now been determined that the toxicity of these mutants relies on their ability to catalyze the formation of a highly toxic peroxynitrate from NO and O^{2-} (*36*, *39*). This property is related to the deficiency of zinc of these mutants. Indeed, Zn-depleted WT SOD is also able to generate peroxynitrate and to cause neuronal apoptosis (*36*). The lack of zinc induces small changes in the copper coordination, which may impart to copper a much higher oxidative capability. Therefore, the conformation of Asp 124 might be essential in determining the affinity of zinc for SOD and for obtaining a fully metalated protein. Indeed, ALS-related mutations are quite extensively found in the Zn binding loop, and even of Asp 124, where the latter mutants are almost completely lacking the zinc ion. These mutations may affect the conformation of Asp 124 and consequently the affinity for zinc.

The observation that this residue experiences a different conformation in solution and in the crystal suggests that it is quite sensitive to its surrounding environment and that its conformation is a fine balance of many factors. Even minor alterations in the protein, as those induced by point mutations, may propagate to this key Asp 124 residue which affects the affinity for zinc and consequently the copper coordination and oxidative properties. The large conformational space available for the Asp 124 side chain allows this residue to behave like a trigger for zinc binding. As for many other structural properties (*19*, *40*), several residues in this enzyme have been organized to assume the optimal conformation for the efficiency of the enzymatic reaction but also for its selectivity.

Finally, these observations tempt us to suggest a more essential role for the zinc ion, i.e., that of maintaining the oxidative capability of the copper ion in SOD in a very specific range and of preventing it from catalyzing further toxic reactions.

ACKNOWLEDGMENT

We are grateful to Maria Silvia Viezzoli for sample preparation and to Helena Kovacs, Detlef Moskau, and Christian Richter from Bruker AG for the access to the cryoprobe. Sheref Mansy is acknowledged for careful reading of the manuscript.

SUPPORTING INFORMATION AVAILABLE

Pulse scheme used to detect hydrogen bonds, a figure showing the ^{15}N TROSY R_2 relaxation rates versus residue number, and a table reporting the $^{3h}J_{NC'}$ coupling constants. This material is available free of charge via the Internet at http://pubs.acs.org.

REFERENCES

1. Loh, S. N., and Markley, J. L. (1994) *Biochemistry 33*, 1029.
2. Dingley, A. J., and Grzesiek, S. (1998) *J. Am. Chem. Soc 120*, 8293−8297.
3. Pervushin, K., Ono, A., Fernandez, C., Szyperski, T., Kainosho, M., and Wüthrich, K. (1998) *Proc. Natl. Acad. Sci. U.S.A. 95*, 14147−14151.
4. Dingley, A. J., Cordier, F., and Grzesiek, S. (2001) *Concepts Magn. Reson. 13*, 103−127.
5. Cordier, F., and Grzesiek, S. (1999) *J. Am. Chem. Soc. 121*, 1601−1602.
6. Corneliescu, G., Hu, J.-S., and Bax, A. (1999) *J. Am. Chem. Soc. 121*, 2949−2950.

7. Corneliescu, G., Ramirez, B. E., Frank, M. K., Clore, G. M., Gronenborn, A. M., and Bax, A. (1999) *J. Am. Chem. Soc. 121*, 6275−6279.
8. Wang, Y. X., Jacob, J., Cordier, F., Wingfield, P., Stahl, S. J., Lee-Huang, S., Torchia, D. A., Grzesiek, S., and Bax, A. (1999) *J. Biomol. NMR 14*, 181−184.
9. Pervushin, K., Riek, R., Wider, G., and Wüthrich, K. (1997) *Proc. Natl. Acad. Sci. U.S.A. 94*, 12366−12371.
10. Fridovich, I. (1986) *Adv. Enzymol. Relat. Areas Mol. Biol. 58*, 61−97.
11. Valentine, J. S., and Pantoliano, M. W. (1981) in *Metal Ions in Biological Systems* (Sigel, H., Ed.) Vol. 3, pp 291−358, Dekker, New York.
12. Bertini, I., Mangani, S., and Viezzoli, M. S. (1998) in *Advanced Inorganic Chemistry* (Sykes, A. G., Ed.) pp 127−250, Academic Press, San Diego.
13. McCord, J. M., and Fridovich, I. (1969) *J. Biol. Chem. 244*, 6049−6055.
14. Fee, J. A., and Gaber, B. P. (1972) *J. Biol. Chem. 247*, 60−65.
15. Tainer, J. A., Getzoff, E. D., Beem, K. M., Richardson, J. S., and Richardson, D. C. (1982) *J. Mol. Biol. 160*, 181−217.
16. Parge, H. E., Hallewell, R. A., and Tainer, J. A. (1992) *Proc. Natl. Acad. Sci. U.S.A. 89*, 6109−6114.
17. Bertini, I., Piccioli, M., Viezzoli, M. S., Chiu, C. Y., and Mullenbach, G. T. (1994) *Eur. J. Biophys. 23*, 167−176.
18. Banci, L., Bertini, I., Chiu, C. Y., Mullenbach, G. T., and Viezzoli, M. S. (1995) *Eur. J. Biochem. 234*, 855−860.
19. Banci, L., Benedetto, M., Bertini, I., Del Conte, R., Piccioli, M., and Viezzoli, M. S. (1998) *Biochemistry 37*, 11780−11791.
20. Banci, L., Bertini, I., Del Conte, R., Mangani, S., and Viezzoli, M. S. (1999) *J. Biol. Inorg. Chem. 4*, 795−803.
21. Banci, L., Bertini, I., Cramaro, F., Del Conte, R., Rosato, A., and Viezzoli, M. S. (2000) *Biochemistry 39*, 9108−9118.
22. Ferraroni, M., Rypniewski, W., Wilson, K. S., Viezzoli, M. S., Banci, L., Bertini, I., and Mangani, S. (1999) *J. Mol. Biol. 288*, 413−426.
23. Banci, L., Benedetto, M., Bertini, I., Del Conte, R., Piccioli, M., Richert, T., and Viezzoli, M. S. (1997) *Magn. Reson. Chem. 35*, 845−853.
24. Getzoff, E. D., Cabelli, D. E., Fisher, C. L., Parge, H. E., Viezzoli, M. S., Banci, L., and Hallewell, R. A. (1992) *Nature 358*, 347−351.
25. Kay, L. E., Ikura, M., Tschudin, R., and Bax, A. (1990) *J. Magn. Reson. 89*, 496−514.
26. Grzesiek, S., and Bax, A. (1992) *J. Magn. Reson. 96*, 432−440.
27. Kay, L. E., Xu, G. Y., and Yamazaki, T. (1994) *J. Magn. Reson., Ser. A 109*, 129−133.
28. Palmer, A. G., III, Cavanagh, J., Wright, P. E., and Rance, M. (1991) *J. Magn. Reson. 93*, 151−170.
29. Emsley, L., and Bodenhausen, G. (1990) *Chem. Phys. Lett. 165*, 469−476.
30. Emsley, L., and Bodenhausen, G. (1992) *J. Magn. Reson. 97*, 135−148.
31. Güntert, P., Mumenthaler, C., and Wüthrich, K. (1997) *J. Mol. Biol. 273*, 283−298.
32. Laskowski, R. A., MacArthur, M. W., Moss, D. S., and Thornton, J. M. (1993) *J. Appl. Crystallogr. 26*, 283−291.
33. Laskowski, R. A., Rullmann, J. A. C., MacArthur, M. W., Kaptein, R., and Thornton, J. M. (1996) *J. Biomol. NMR 8*, 477−486.
34. Hough, M. A., Strange, R. W., and Hasnain, S. S. (2000) *J. Mol. Biol. 304*, 231−241.
35. Banci, L., Bertini, I., Cabelli, D. E., Hallewell, R. A., Tung, J. W., and Viezzoli, M. S. (1991) *Eur. J. Biochem. 196*, 123−128.
36. Estévez, A. G., Crow, J. P., Sampson, J. B., Reiter, C., Zhuang, Y., Richardson, G. J., Tarpey, M. M., Barbeito, L., and Beckman, J. S. (1999) *Science 286*, 5449.
37. Goto, J. J., Zhu, H., Sanchez, R. J., Nerissian, A., Gralla, E. B., and Valentine, J. S. (2000) *J. Biol. Chem. 275*, 1007−1014.
38. Lyons, T. J., Nerissian, A., Huang, H., Yeom, H., Nishida, C. R., Graden, J. A., Gralla, E. B., and Valentine, J. S. (2000) *J. Biol. Inorg. Chem. 5*, 189−203.
39. Crow, J. P., Sampson, J. B., Zhuang, Y., Thomson, J. A., and Beckman, J. S. (1997) *J. Neurochem. 69*, 1936−1944.
40. Banci, L., Bertini, I., Del Conte, R., and Viezzoli, M. S. (1999) *Biospectroscopy 5*, 33−41.
41. Koradi, R., Billeter, M., and Wüthrich, K. (1996) *J. Mol. Graphics 14*, 51−55.

BI011617B